CC BY

A Magnetically Recyclable Fe_3O_4/GO/Chitosan Nanocomposite for Water Decontamination and Electrocatalytic Hydrogen Evolution

M. Mohamed Ismail[1], A. Sankar[2]

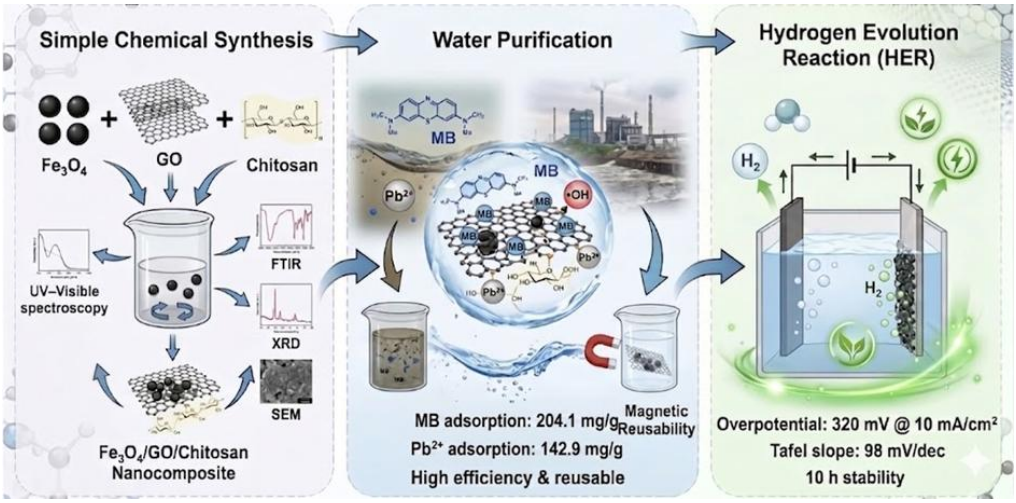
Abstract

Water pollution caused by industrial waste, dyes, and heavy metals has become a major environmental concern worldwide. In this study, a nanocomposite material was synthesized and characterized for its potential application in water purification and clean energy generation. The nanocomposite was prepared using a simple chemical synthesis method to combine the advantageous properties of iron oxide nanoparticles, graphene oxide, and chitosan. The synthesized material was characterized using various analytical techniques such as UV–Visible spectroscopy, Fourier Transform Infrared Spectroscopy (FTIR), X-ray Diffraction (XRD), and Scanning Electron Microscopy (SEM) to determine its structural, optical, and surface properties. The characterization results confirmed the successful formation of the nanocomposite with good surface morphology, magnetic responsiveness, and stability. The prepared nanocomposite was evaluated for the removal of pollutants from contaminated water through adsorption and catalytic activity, and separately for its electrocatalytic performance toward the hydrogen evolution reaction (HER). Experimental results indicated that the material showed effective purification performance with improved removal efficiency and reusability, achieving maximum adsorption capacities of 204.1 mg/g for methylene blue and 142.9 mg/g for Pb^{2+} ions. Furthermore, the nanocomposite exhibited an overpotential of 320 mV at 10 mA/cm² for HER with a Tafel slope of 98 mV/dec and stable operation for 10 hours. The study demonstrates that this nanocomposite material can serve as a promising and environmentally friendly candidate for advanced water treatment applications and as a low-cost electrocatalyst for hydrogen production.

[1,2]Department of Chemistry, Kandaswami Kandar's College (Affiliated to Periyar University, Salem), P. Velur, Namakkal Dt, Tamilnadu, India. (ismail.try3503@gmail.com)

*Corresponding author

Graphical Abstract



Introduction

The rapid pace of industrialization has brought with it a troubling legacy of water pollution. Factories discharge wastewater containing a bewildering variety of chemical contaminants, among which synthetic dyes and heavy metals are particularly problematic. Methylene blue, a common dye used in textile and paper industries, colors water even at very low concentrations, blocking sunlight and harming aquatic life. Heavy metals like lead accumulate in the food chain and cause irreversible damage to human health, including developmental disorders in children and kidney failure in adults. Traditional water treatment methods struggle to remove these pollutants effectively. Coagulation and flocculation work well for suspended solids but leave dissolved contaminants untouched. Activated carbon adsorption is effective but expensive to regenerate. Membrane filtration requires high energy inputs and produces concentrated waste streams. Advanced oxidation processes using ozone or hydrogen peroxide can destroy organic pollutants, but they consume significant amounts of energy and chemicals. What is needed are new materials that are inexpensive, easy to recover, and capable of handling multiple types of pollutants. At the same time, the world is searching for clean alternatives to fossil fuels. Hydrogen is an ideal energy carrier because burning it produces only water. However, most hydrogen today comes from natural gas through steam methane reforming, a process that releases large amounts of carbon dioxide. Splitting water into hydrogen and oxygen using electricity offers a clean pathway, especially when the electricity comes from renewable sources. The challenge is that water splitting requires a catalyst to speed up the hydrogen-producing reaction. Platinum is an excellent catalyst but is far too expensive and rare for large-scale use. Finding abundant, low-cost materials that can catalyze hydrogen evolution is therefore an active area of research.

Nanomaterials have opened new possibilities for both water treatment and catalysis. Their tiny size gives them enormous surface areas relative to their mass, meaning more active sites are available for binding pollutants or catalyzing reactions. Iron oxide in the form of magnetite (Fe_3O_4) is particularly attractive because it is magnetic, which allows easy separation from water, and it also has catalytic properties. However, bare iron oxide nanoparticles tend to clump together, reducing their effectiveness. They also conduct electricity poorly, limiting their use in electrochemical applications. Attaching iron oxide nanoparticles to a supporting material can overcome these problems. Graphene oxide consists of single-atom-thick carbon sheets covered with oxygen-containing functional groups. These sheets provide a large, flat surface for anchoring nanoparticles, and the oxygen groups can themselves bind pollutant molecules. Chitosan is a natural polymer obtained from crab and shrimp shells. It is biodegradable, non-toxic, and contains amine groups that strongly bind heavy metals. Combining these three materials into a single composite could produce a versatile material that works well for both water cleanup and hydrogen production. The present study describes the synthesis of a

composite containing iron oxide nanoparticles, graphene oxide sheets, and chitosan using a simple one-pot co-precipitation method. The material was thoroughly characterized using several analytical techniques. Its ability to remove methylene blue and lead ions from water was evaluated through batch adsorption experiments. Its catalytic activity for breaking down methylene blue in the presence of hydrogen peroxide was also tested. Separately, its performance as an electrocatalyst for hydrogen evolution was measured using standard electrochemical methods. The ease of recovering the material with a magnet and reusing it over multiple cycles was assessed for both applications.

Experimental Section

Chemicals and Reagents

All chemicals were of analytical grade and used without further purification. Graphite powder (≤20 µm, 99.9%), potassium permanganate ($KMnO_4$, ≥99%), concentrated sulfuric acid (98%), hydrogen peroxide (30%), ferric chloride hexahydrate ($FeCl_3 \cdot 6H_2O$, 97%), ferrous sulfate heptahydrate ($FeSO_4 \cdot 7H_2O$, 99%), chitosan (low molecular weight, 75–85% deacetylated), glacial acetic acid (99.7%), sodium hydroxide (98%), methylene blue ($C_{16}H_{18}ClN_3S$, ≥82%), lead nitrate ($Pb(NO_3)_2$, 99%), hydrochloric acid (37%), and sulfuric acid (95–98%) were obtained from Merck and Sigma-Aldrich. Deionized water with a resistivity of 18.2 MΩ·cm was produced by a Milli-Q water purification system and used throughout.

Synthesis of Graphene Oxide

Graphene oxide was prepared using a modified Hummers method. In a typical procedure, 3.0 g of graphite powder was added to 150 mL of concentrated H_2SO_4 in a 1 L round-bottom flask immersed in an ice bath. The mixture was stirred for 30 minutes to ensure thorough mixing. Then, 18.0 g of $KMnO_4$ was added slowly in small portions over 1 hour, keeping the temperature below 20 °C to prevent overheating. After complete addition, the ice bath was removed, and the mixture was heated to 35 °C and stirred for 2 hours, during which time the color changed from dark green to a thick brown paste. Next, 250 mL of deionized water was added dropwise with vigorous stirring, causing the temperature to rise to approximately 90 °C. The mixture was then diluted with a further 500 mL of warm water (50 °C), and 30 mL of 30% H_2O_2 was added dropwise, turning the solution bright yellow. The resulting GO suspension was centrifuged at 8,000 rpm for 15 minutes, washed sequentially with 200 mL of 5% HCl solution and then with deionized water until the pH reached 6.0, and finally freeze-dried for 48 hours to obtain a fluffy, light brown solid.

Synthesis of Fe_3O_4/GO/Chitosan Nanocomposite

The ternary nanocomposite was prepared using an insitu co-precipitation method. 200 mg of freeze-dried GO was dispersed in 100 mL of deionized water by ultrasonication (150 W, 40 kHz) for 1 hour. Separately, 0.5 g of chitosan was dissolved in 50 mL of 1% (v/v) acetic acid under magnetic stirring for 2 hours. The chitosan solution was then added to the GO dispersion, and the mixture was stirred for an additional hour to allow electrostatic interactions. The pH of the combined mixture was adjusted to approximately 4.5 using 0.1 M NaOH. In a separate beaker, 0.01 mol (2.70 g) of $FeCl_3 \cdot 6H_2O$ and 0.005 mol (1.39 g) of $FeSO_4 \cdot 7H_2O$ were dissolved in 50 mL of deionized water (Fe^{3+}:Fe^{2+} molar ratio = 2:1). This iron salt solution was added dropwise to the GO/chitosan mixture under vigorous stirring at 80 °C. After 30 minutes, 25% ammonium hydroxide solution was added dropwise until the pH reached 10.5, triggering the immediate co-precipitation of Fe_3O_4 nanoparticles. The temperature was maintained at 80 °C for an additional 2 hours under continuous stirring. The resulting black precipitate was separated using a neodymium magnet, washed three times with deionized water and three times with ethanol, and dried in a vacuum oven at 60 °C for 12 hours. For comparison, bare Fe_3O_4 nanoparticles were synthesized using the same method without GO and chitosan. The diagrammatic representation of synthesis scheme is shown in Figure 1.

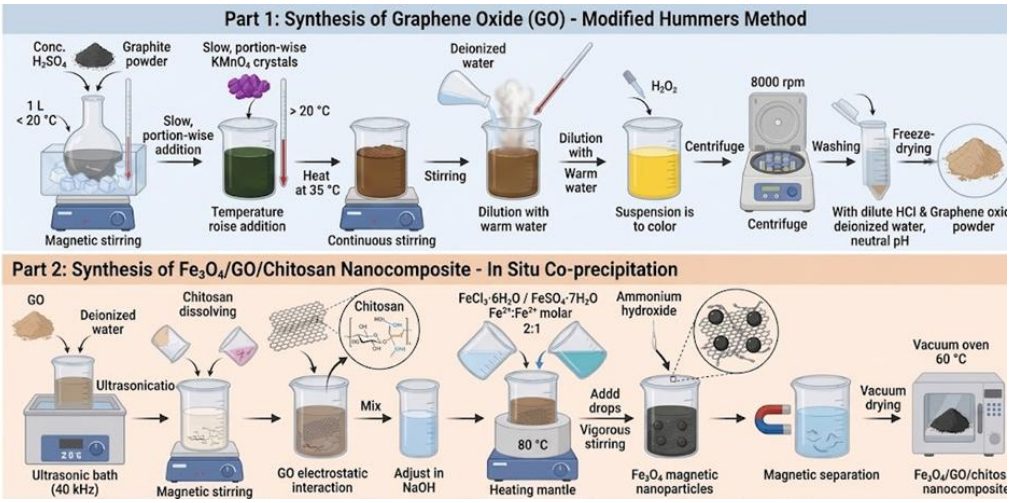


Figure 1. Multi-Step Synthesis of Graphene Oxide (GO) and Ternary Nanocomposite through in situ Co-precipitation technique.

Characterization Techniques

UV-Visible absorption spectra were recorded on a Shimadzu UV-2600 spectrophotometer over the range of 200–800 nm. For solid samples, approximately 5 mg of powder was dispersed in 5 mL of deionized water by sonication and transferred to a quartz cuvette. Fourier Transform Infrared Spectroscopy (FTIR) was performed using a PerkinElmer Spectrum Two spectrometer equipped with an attenuated total reflectance (ATR) accessory. Approximately 5 mg of each powdered sample was placed directly onto the diamond crystal, and spectra were collected from 4000 to 400 cm^{-1} at a resolution of 4 cm^{-1}, with 32 scans co-added. X-ray Diffraction (XRD) patterns were obtained using a Bruker D8 Advance diffractometer with Cu-Kα radiation (λ = 1.5406 Å). The X-ray tube was operated at 40 kV and 40 mA. Powder samples were scanned over a 2θ range of 10° to 80° with a step size of 0.02° and a scan speed of 2° per minute. The average crystallite size of the Fe_3O_4 phase was estimated using the Scherrer equation. Scanning Electron Microscopy (SEM) was performed on a Zeiss EVO MA 10 instrument. Powder samples were mounted on aluminum stubs using double-sided carbon tape and sputter-coated with a thin layer of gold (≈5 nm) to prevent charging. Images were acquired at an accelerating voltage of 15 kV using the secondary electron detector. Energy-dispersive X-ray (EDX) analysis was performed using an Oxford Instruments detector. Magnetic properties were measured at room temperature using a Lakeshore 7407 vibrating sample magnetometer (VSM). Approximately 20 mg of dried powder was placed in a gelatin capsule, and the magnetic field was swept from –15 kOe to +15 kOe.

Batch Adsorption Experiments

All adsorption experiments were conducted in 250 mL Erlenmeyer flasks placed on an orbital shaker at 200 rpm, with the temperature maintained at 25 ± 1 °C. In each experiment, 20 mg of nanocomposite was added to 50 mL of solution containing either methylene blue or Pb^{2+} ions at the desired initial concentration. After the prescribed contact time, the nanocomposite was separated by placing a neodymium magnet against the side of the flask for 30 seconds, and the supernatant was decanted for analysis. For pH optimization, the initial pH of the pollutant solution was adjusted from 2 to 10 using 0.1 M HCl or 0.1 M NaOH. The initial pollutant concentration was 50 mg/L, and the contact time was 120 minutes. The removal efficiency was calculated as $(C_0 - C)/C_0 \times 100\%$. Kinetic experiments were performed at the optimal pH (pH 8 for methylene blue and pH 5 for Pb^{2+}) with an initial concentration of 50 mg/L. Samples were taken at 0, 5, 10, 15, 30, 45, 60, 90, 120, 150, and 180 minutes. The amount adsorbed at time t, q_t (mg/g), was calculated using the mass balance equation: $q_t = (C_0 - C_t)V/m$. Kinetic data were fitted to pseudo-first-order and pseudo-second-order models. Isotherm experiments were conducted by varying the initial pollutant concentration from 10 to 200 mg/L for methylene blue and from 5 to 150 mg/L for Pb^{2+}, with a contact time of 180 minutes to

ensure equilibrium. The equilibrium concentration (C_e) and equilibrium adsorption capacity (q_e) were determined. Data were fitted to the Langmuir and Freundlich isotherm models. Methylene blue concentration was measured by UV-Vis absorbance at 664 nm using a calibration curve. Pb^{2+} concentration was measured using a PerkinElmer AAnalyst 200 atomic absorption spectrometer at 283.3 nm.

Catalytic Degradation of Methylene Blue

To assess the ability of the prepared nanocomposite to break down organic pollutants, a series of Fenton-like catalytic experiments were carried out, focusing specifically on the oxidative degradation of methylene blue, which served as a model dye contaminant. In each standard test, 10 milligrams of the nanocomposite were mixed into 50 milliliters of a methylene blue solution that had an initial concentration of 20 milligrams per liter. The pH of this mixture was then carefully brought down to 3.0 by adding small amounts of 0.1 molar sulfuric acid. This specific acidic condition was chosen because it is well established in Fenton-like chemistry to be the most effective for generating highly reactive hydroxyl radicals, which are the primary species responsible for attacking and breaking down organic dye molecules. Once the pH was stabilized, the degradation reaction was officially started by adding hydrogen peroxide to the mixture so that its final concentration reached 5 millimolar. Over the course of the reaction, small samples of 1 milliliter each were taken out at set time points: right at the beginning, and then after 5, 10, 15, 20, 30, 45, and 60 minutes. Immediately after each sample was collected, an external magnet was used to quickly pull the nanocomposite particles out of the liquid, which effectively stopped any further catalytic reaction from taking place. The clear liquid left behind was then analyzed to find out how much methylene blue remained. This was done by measuring the absorbance of the solution at a wavelength of 664 nanometers, which is the wavelength where methylene blue shows its strongest light absorption. The degradation efficiency was then calculated using a simple formula: the difference between the initial absorbance and the absorbance at a given time, divided by the initial absorbance, and finally multiplied by one hundred percent to get a percentage value.

To make sure the results truly reflected the catalytic power of the nanocomposite and not some other unrelated effect, several control experiments were run side by side under exactly the same conditions. One control used only hydrogen peroxide without any catalyst to see how much degradation could occur through peroxide alone. Another control used only the nanocomposite without adding hydrogen peroxide to measure how much of the dye was simply adsorbed onto the material's surface rather than being chemically broken down. A third control used plain iron oxide nanoparticles together with hydrogen peroxide, which helped establish the baseline activity coming just from the iron oxide component without any contribution from the graphene oxide or chitosan in the composite. These control experiments were essential because they allowed a clear distinction between true oxidative degradation and mere physical adsorption. They also helped confirm that the nanocomposite as a whole performed better than just the sum of its parts. A clear and systematic diagram showing every step of this experimental procedure, from the initial mixing of the nanocomposite with the dye solution to the final absorbance measurement and calculation of degradation efficiency, is provided in Figure 2.

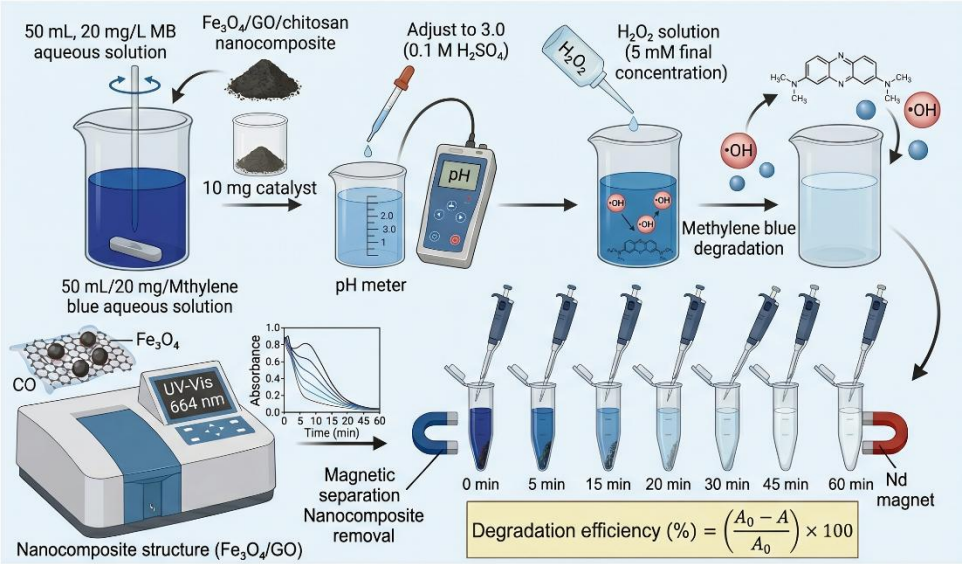


Figure 2. Systematic procedure for the Fenton-like catalytic degradation of Methylene Blue (MB) using an Fe_3O_4/GO/chitosan nanocomposite.

Hydrogen Evolution Reaction (HER) Measurements

Electrochemical measurements were performed using a CH Instruments 660E electrochemical workstation with a standard three-electrode configuration. A glassy carbon electrode (GCE) with a diameter of 3 mm (geometric surface area of 0.0707 cm^2) served as the working electrode. A platinum wire was used as the counter electrode, and a saturated calomel electrode (SCE) was used as the reference electrode. All potentials were converted to the reversible hydrogen electrode (RHE) scale using the equation: E(RHE) = E(SCE) + 0.241 + 0.059 × pH. The electrolyte was 0.5 M H_2SO_4 (pH ≈ 0.3), which was deaerated by bubbling high-purity nitrogen gas for 30 minutes before each measurement. To prepare the working electrode, 2 mg of nanocomposite was dispersed in 1 mL of a solution containing 0.5% Nafion in a mixture of water and ethanol (1:1 v/v). The dispersion was sonicated for 30 minutes, and 5 µL was drop-cast onto the polished glassy carbon electrode surface and dried under an infrared lamp (catalyst loading ≈0.14 mg/cm^2). For comparison, electrodes were prepared using bare Fe_3O_4 and a physical mixture of GO and chitosan. Linear sweep voltammetry (LSV) was performed from 0 V to –0.8 V vs. SCE at a scan rate of 5 mV/s. The overpotential (η) required to achieve a current density of 10 mA/cm^2 was recorded. Tafel plots were constructed by plotting overpotential against the logarithm of current density (log|j|) in the low-overpotential region. Electrochemical impedance spectroscopy (EIS) was performed at –0.3 V vs. RHE over a frequency range of 100 kHz to 0.1 Hz with an AC amplitude of 5 mV. Stability was evaluated by chronopotentiometry at a constant current density of 10 mA/cm^2 for 10 hours.

Reusability Study

For adsorption experiments, after each cycle the pollutant-loaded nanocomposite was separated magnetically, washed twice with 10 mL of deionized water, and desorbed using 20 mL of ethanol (for methylene blue) or 0.1 M HCl (for Pb^{2+}) for 60 minutes. The regenerated nanocomposite was then used in a subsequent adsorption cycle under identical conditions (50 mL of 50 mg/L pollutant, 20 mg nanocomposite, 120 min contact time). Five consecutive cycles were performed. For catalytic degradation, the nanocomposite was recovered magnetically after each run, washed with deionized water, and reused in a fresh 20 mg/L methylene blue solution with 5 mM H_2O_2 at pH 3.0.

Results and Discussion

Structural, Optical, and Magnetic Characterization

The UV-Vis absorption spectra gave the first hints that the composite had formed successfully. When

we looked at graphene oxide by itself, it showed a strong, sharp peak at 230 nanometers, which comes from π→π transitions in the aromatic C=C bonds. There was also a small shoulder around 300 nanometers, due to n→π transitions in the C=O groups. Bare Fe_3O_4 nanoparticles, on the other hand, produced a broad, featureless absorption that simply decreased gradually as we moved from the ultraviolet into the visible region. The nanocomposite spectrum looked different: the main peak shifted slightly to a longer wavelength, appearing at 232 nanometers, and the baseline in the visible region was higher. This told us that there is some electronic interaction happening between Fe_3O_4 and GO. When we estimated the optical bandgap using Tauc plots, we found that the nanocomposite had a bandgap of 2.8 electron volts, which is lower than that of bare Fe_3O_4 at 3.1 electron volts. This lower bandgap means the composite can absorb more visible light, which is a desirable property for many applications.

Moving to FTIR spectroscopy, we got clear evidence that all three components were chemically integrated with each other. In the GO spectrum, we saw a band at 3420 reciprocal centimeters for O–H stretching, another at 1725 for C=O stretching of carboxylic acids, one at 1620 for C=C stretching, a band at 1220 for C–O–C epoxy stretching, and another at 1050 for C–O alkoxy stretching. Chitosan gave its own set of bands: a broad one at 3360 from overlapping O–H and N–H stretches, a band at 2875 from aliphatic C–H stretching, one at 1655 for amide I, and a band at 1595 for N–H bending. When we looked at the nanocomposite spectrum, we noticed some important shifts. The C=O peak moved down to 1705, and the N–H bending band shifted to 1575. These shifts indicate electrostatic interactions between the carboxyl groups of GO and the protonated amine groups of chitosan. We also saw a new band appear at 580, which we assigned to the Fe–O stretching of Fe_3O_4, confirming that the magnetite nanoparticles were indeed present in the composite.

The XRD patterns confirmed that the magnetite phase remained crystalline. Bare Fe_3O_4 gave six distinct peaks at 2θ angles of 30.1°, 35.5°, 43.2°, 53.6°, 57.1°, and 62.7°. These correspond to the (220), (311), (400), (422), (511), and (440) planes of cubic spinel Fe_3O_4, matching JCPDS card number 19-0629. The nanocomposite showed exactly the same six peaks without any extra phases, which tells us the material is phase pure. Importantly, the characteristic GO peak at 10.8° was completely missing in the nanocomposite, meaning that the GO sheets had been exfoliated. Using the Scherrer equation on the (311) peak, we calculated the average crystallite size of Fe_3O_4 in the nanocomposite to be 12.5 ± 1.2 nanometers, compared to 18.3 ± 1.5 nanometers for bare Fe_3O_4. This reduction shows that the GO and chitosan matrix effectively prevented the nanoparticles from growing too large and also stopped them from aggregating.

When we examined the material with SEM, we saw a highly porous three-dimensional network structure. The GO sheets appeared as wrinkled, thin layers that were uniformly coated with chitosan, and the Fe_3O_4 nanoparticles, measuring about 15 to 20 nanometers in diameter, were spread homogeneously throughout without forming large clumps. EDX analysis gave us the elemental composition: 38.2 weight percent carbon, 42.5 weight percent oxygen, 17.8 weight percent iron, and 1.5 weight percent nitrogen. The presence of nitrogen confirmed that chitosan was indeed part of the composite.

Finally, VSM measurements revealed that the material is superparamagnetic, meaning it showed zero remanence and zero coercivity. The saturation magnetization of bare Fe_3O_4 was 68.5 emu per gram, while the nanocomposite gave a value of 32.6 emu per gram. This lower value is still more than enough for rapid magnetic separation. To test this, we placed a magnet next to a vial containing the dispersed nanocomposite, and complete separation was achieved within 30 seconds. The structural and optical characterization results of the materials are shown in Figure 3.

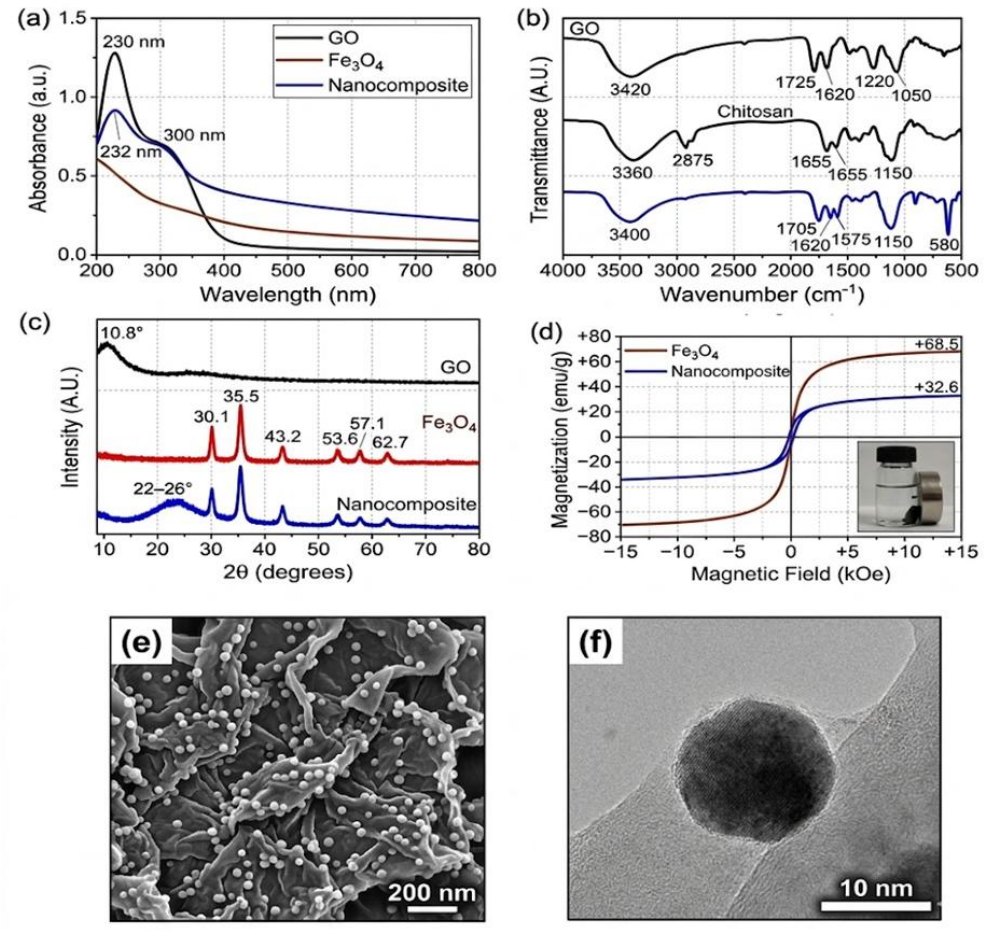


Figure 3. (a) UV-Vis spectra, (b) FTIR spectra, (c) XRD patterns, and (d) magnetic hysteresis loops of GO, bare Fe_3O_4, and the nanocomposite, confirming successful formation and superparamagnetic behavior. (e) SEM image (200 nm scale bar) showing porous structure with uniform Fe_3O_4 dispersion on GO sheets. (f) HR-TEM image (10 nm scale bar) showing lattice fringes of a single Fe_3O_4 nanoparticle (d = 0.25 nm) anchored on a wrinkled GO sheet.

Adsorption Performance for Water Pollutants

The initial pH strongly influenced adsorption. For methylene blue, removal efficiency increased from 22% at pH 2 to 94% at pH 8 and 96% at pH 10. The point of zero charge (pH_{pzc}) of the nanocomposite was determined to be approximately 6.2. Below this pH, the surface is positively charged, repelling the cationic dye; above pH_{pzc}, the surface becomes negatively charged, attracting the dye. For Pb^{2+}, maximum removal (98%) occurred at pH 5, with decreasing removal at higher pH due to $Pb(OH)_2$ precipitation. Therefore, pH 5 was used for all lead experiments.

Adsorption kinetics showed rapid uptake during the first 30 minutes, followed by a slower approach to equilibrium. Equilibrium was reached at 120 minutes for methylene blue and 150 minutes for Pb^{2+}. The pseudo-second-order model provided excellent fits for both pollutants ($R^2 = 0.998$ for MB, $R^2 = 0.996$ for Pb^{2+}), with calculated equilibrium capacities (q_e) of 119.5 mg/g (MB) and 86.3 mg/g (Pb^{2+}) matching experimental values closely. This indicates that chemisorption is the rate-limiting step.

Adsorption isotherms were best described by the Langmuir model, suggesting monolayer adsorption on a homogeneous surface. The maximum Langmuir adsorption capacities (q_{max}) were 204.1 mg/g for methylene blue and 142.9 mg/g for Pb^{2+}. These values are superior to many previously reported magnetic graphene-based adsorbents, attributed to the high surface area of exfoliated GO, abundant

functional groups, and uniform Fe_3O_4 dispersion. The adsorption behavior of the nanocomposite for methylene blue and Pb^{2+} is depicted in Figure 4.

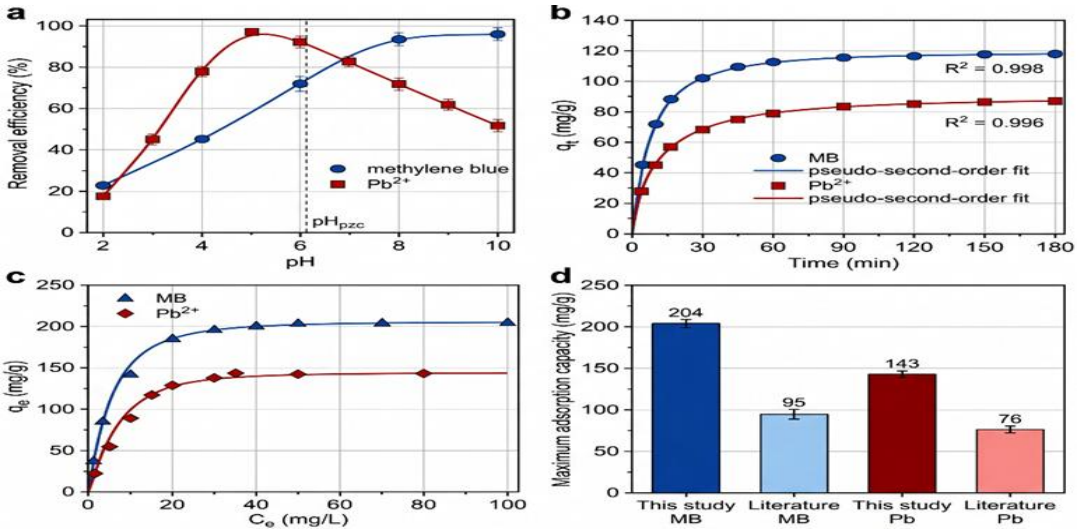


Figure 4. Four-panel figure showing the adsorption behavior of the nanocomposite for methylene blue and Pb^{2+}. (a) Effect of pH on removal efficiency, (b) adsorption kinetics with pseudo-second-order fits, (c) Langmuir adsorption isotherms, and (d) comparison of maximum adsorption capacities with literature values for methylene blue and Pb^{2+}.

Catalytic Degradation of Methylene Blue

In the Fenton-like experiments, hydrogen peroxide by itself was barely effective, degrading less than 5% of methylene blue over the course of 60 minutes. When the nanocomposite was used alone without any hydrogen peroxide, only 12% of the dye was removed, and that removal was due solely to adsorption rather than any chemical breakdown. However, when the complete system combining the nanocomposite with hydrogen peroxide was tested, a dramatic improvement was observed: 92% of the methylene blue was degraded within just 45 minutes. This reaction followed pseudo first order kinetics, with a rate constant calculated as 0.058 per minute and an R squared value of 0.99, indicating an excellent fit to the model. For comparison, bare Fe_3O_4 nanoparticles tested with hydrogen peroxide reached only 72% degradation after 60 minutes, clearly showing that the graphene oxide and chitosan matrix surrounding the iron oxide particles plays a crucial role in boosting the catalytic performance.

The underlying mechanism begins with ferrous iron sites, or Fe^{2+}, located on the surface of the magnetite nanoparticles. These Fe^{2+} sites react with hydrogen peroxide to generate highly reactive hydroxyl radicals, following the classic Fenton reaction: Fe^{2+} plus H_2O_2 produces Fe^{3+}, a hydroxyl radical, and a hydroxide ion. The hydroxyl radicals are extremely powerful and non selective oxidants; they attack the methylene blue molecule, breaking its aromatic ring structures and eventually converting the dye into carbon dioxide, water, and other small inorganic products, a process known as mineralization. What makes the nanocomposite particularly effective is the presence of graphene oxide, which acts as an electron shuttle. It facilitates the reduction of ferric iron, or Fe^{3+}, back to ferrous iron, or Fe^{2+}, thereby sustaining the Fenton cycle and preventing the catalytic activity from dying out quickly. This continuous regeneration of active iron sites explains why the nanocomposite outperforms bare Fe_3O_4 nanoparticles. Figure 5 visually illustrates this catalytic activity of the nanocomposite throughout the reaction process.

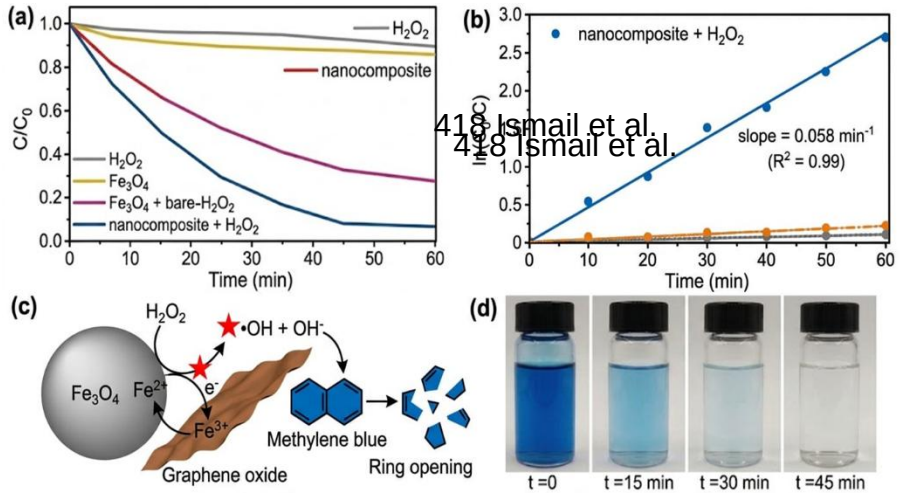


Figure 5. Four-panel figure showing the Fenton-like catalytic activity of the nanocomposite. (a) Time-dependent degradation of methylene blue under different conditions, (b) pseudo-first-order kinetic plot, (c) schematic of the Fenton-like degradation mechanism, and (d) photographs showing the progressive decolorization of the dye solution.

Hydrogen Evolution Reaction Performance

The nanocomposite exhibited promising hydrogen evolution reaction (HER) activity in 0.5 M H_2SO_4, as systematically evaluated through linear sweep voltammetry (LSV). It required an overpotential (η_{10}) of only 320 mV to achieve a current density of 10 mA/cm², a benchmark value commonly used to compare HER catalysts. In stark contrast, bare Fe_3O_4 demanded a substantially higher overpotential of 580 mV, while the GO/chitosan mixture displayed negligible HER activity, with an η_{10} exceeding 700 mV. This significant reduction in overpotential underscores a synergistic effect introduced by the nanocomposite architecture, wherein the components collectively enhance catalytic performance beyond their individual contributions. Further kinetic analysis derived from Tafel plots revealed a Tafel slope of 98 mV/dec for the nanocomposite, indicating a Volmer–Heyrovsky mechanism in which the electrochemical desorption step is rate-determining. Compared to bare Fe_3O_4, which showed a Tafel slope of 145 mV/dec, the nanocomposite's lower Tafel slope suggests markedly faster reaction kinetics and a more favorable HER pathway efficiency. A steeper Tafel slope typically implies a kinetically sluggish process; thus, the observed reduction of nearly 50 mV/dec reflects that the incorporation of GO and chitosan into the Fe_3O_4 matrix effectively accelerates hydrogen evolution by optimizing the surface adsorption and electron-transfer characteristics.

Electrochemical impedance spectroscopy (EIS) corroborated these findings by probing the interfacial charge transport properties of the materials. The nanocomposite presented a much smaller charge transfer resistance (R_t) of 45 Ω relative to that of bare Fe_3O_4, which exhibited a substantially larger R_t of 210 Ω. This substantial reduction in charge transfer resistance indicates faster electron transfer from the electrode surface to the catalyst, a critical factor for efficient electrocatalysis. The enhancement is primarily attributed to the presence of a conductive graphene oxide (GO) network within the composite; this conductive framework not only facilitates rapid electron transport pathways but also mitigates ohmic resistive losses that typically hinder catalytic activity in semiconducting metal oxides like Fe_3O_4. Long-term stability was assessed via chronopotentiometry at a constant current density of 10 mA/cm² over 10 hours. The nanocomposite demonstrated excellent durability, with only a modest overpotential increase from 320 mV to 358 mV corresponding to 12% rise. This low degree of degradation highlights the robust structural and chemical integrity of the nanocomposite under prolonged electrochemical operation. A diagrammatic representation summarizing the electrocatalytic HER activity of the nanocomposite is provided in Figure 6.

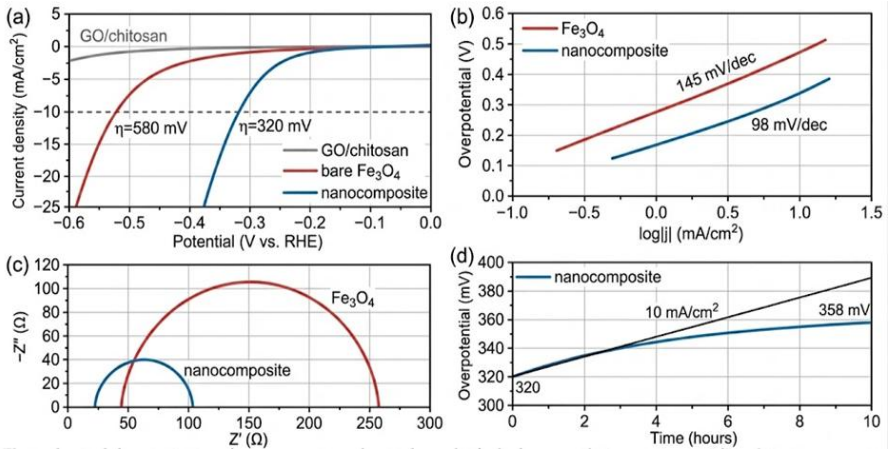


Figure 6. Four-panel figure showing the electrocatalytic HER activity of the nanocomposite. (a) Linear sweep voltammetry polarization curves, (b) Tafel plots, (c) Nyquist plots from electrochemical impedance spectroscopy, and (d) chronopotentiometry stability test at 10 mA/cm² for 10 hours.

Reusability

Over five consecutive adsorption–desorption cycles, the removal efficiency of methylene blue decreased from 96.2% (cycle 1) to 86.5% (cycle 5), while Pb^{2+} removal decreased from 95.8% to 81.3%. For catalytic degradation, efficiency decreased from 92% (cycle 1) to 78% (cycle 5). Magnetic recovery remained above 95% in all cycles. The gradual decline is attributed to incomplete desorption of strongly bound pollutants and slight oxidation of Fe_3O_4 surface sites. Nevertheless, the material retains substantial activity after five cycles, confirming its suitability for repeated use.

Discussion

The Fe_3O_4/GO/chitosan nanocomposite successfully integrates the complementary properties of its three components. The synthesis is straightforward, aqueous-based, and scalable. Characterization confirms small (12.5 nm), well-dispersed Fe_3O_4 nanoparticles anchored to exfoliated GO sheets within a porous chitosan matrix. The magnetic properties enable rapid separation, a critical practical advantage. For water purification, the material achieves excellent adsorption capacities (204 mg/g for MB, 143 mg/g for Pb^{2+}) that compare favorably with the literature. The fast kinetics (equilibrium within 2–2.5 hours) and good reusability (five cycles with <15% loss) further support its potential for real-world applications. The additional Fenton-like catalytic activity (92% degradation in 45 minutes) offers a pathway for destroying organic pollutants rather than merely transferring them to a solid phase. For hydrogen evolution, the nanocomposite delivers an overpotential of 320 mV at 10 mA/cm², a Tafel slope of 98 mV/dec, and stable operation for 10 hours. While not matching platinum, these values are competitive with many non-precious metal HER catalysts. The same Fe_3O_4 nanoparticles that catalyze Fenton reactions also catalyze HER, and the GO sheets provide the electrical conductivity needed for electrocatalysis. A limitation is that HER measurements were performed in acidic electrolyte, while water treatment typically occurs at near-neutral pH. Future work should explore HER performance in neutral or alkaline conditions and investigate the possibility of using the same material sequentially for water purification followed by hydrogen production from the treated water.

Conclusion

In this study, a Fe_3O_4/GO/chitosan nanocomposite was successfully synthesized using a simple one-pot co-precipitation method. Characterization by UV-Vis, FTIR, XRD, and SEM confirmed the formation of a stable, porous, magnetic material with 12.5 nm Fe_3O_4 nanoparticles uniformly dispersed on exfoliated GO sheets within a chitosan matrix. The nanocomposite demonstrated excellent performance for water purification: maximum Langmuir adsorption capacities of 204 mg/g for methylene blue and 143 mg/g for Pb^{2+}, rapid adsorption kinetics following the pseudo-second-

order model, and 92% Fenton-like catalytic degradation of methylene blue in 45 minutes. The material was easily recovered by magnetic separation within 30 seconds and maintained good performance over five reuse cycles. Furthermore, the nanocomposite showed promising electrocatalytic activity for the hydrogen evolution reaction, with an overpotential of 320 mV at 10 mA/cm², a Tafel slope of 98 mV/dec, and stable operation for 10 hours. This dual functionality—water purification and hydrogen evolution—in a single, low-cost, environmentally friendly material represents a significant advance toward integrated solutions for environmental remediation and sustainable energy production.

References

1. Hummers, W. S., & Offeman, R. E. (1958). Preparation of graphitic oxide. Journal of the American Chemical Society, 80(6), 1339–1339. https://doi.org/10.1021/ja01539a017

2. Zhang, Z., Lu, B., Hao, J., Yang, W., & Tang, J. (2014). FeP nanoparticles grown on graphene sheets as highly active non-precious-metal electrocatalysts for hydrogen evolution reaction. Chemical Communications, 50(78), 11554–11557. https://doi.org/10.1039/C4CC05285D

3. Fan, L., Luo, C., Sun, M., Li, X., & Qiu, H. (2013). Highly selective adsorption of Pb^{2+} by a magnetic graphene oxide/chitosan composite. Bioresource Technology, 146, 179–184. https://doi.org/10.1016/j.biortech.2013.07.063

4. Gul, K., Sohni, S., Waqar, M., Ahmad, F., Norulaini, N. A. N., & A. K., M. O. (2016). Functionalization of magnetic chitosan with graphene oxide for removal of cationic and anionic dyes from aqueous solution. Carbohydrate Polymers, 152, 520–531.

   https://doi.org/10.1016/j.carbpol.2016.06.045

5. Lai, K. C., Hiew, B. Y. Z., Lee, L. Y., Gan, S., Thangalazhy-Gopakumar, S., Chiu, W. S., & Khiew, P. S. (2019). Ice-templated graphene oxide/chitosan aerogel as an effective adsorbent for sequestration of metanil yellow dye. Bioresource Technology, 274, 134–144

   https://doi.org/10.1016/j.biortech.2018.11.048

6. Thakur, M., Singh, H., Rajput, J. K., & Kumar, R. (2023). Morphological and structural analysis of Fe/Sn bimetal system and graphene oxide–chitosan modified Fe/Sn composite: a comparative study and their mechanistic role in degradative fixation of chlorazol black and reactive blue 4 from water. Reaction Kinetics, Mechanisms and Catalysis, 136(2), 689–711. https://doi.org/10.1007/s11144-023-02356-

7. Thakur, M., Rajput, J. K., & Kumar, R. (2023). Study of morphological aspects in the efficient adsorptive removal of heavy metal ions using graphene oxide-chitosan based magnetic nanocomposite (0.4Fe0x:6x@GCS). Journal of Hazardous Materials Advances, 10, 100362. https://doi.org/10.1016/j.hazadv.2023.100362

8. Xue, Z., Deng, X., Li, J., Yu, Y., Zhu, Q., Yan, Q., Cui, J., Zuo, X., & Liang, H. (2025). In situ embedding of Fe_3O_4 into large-lateral graphene oxide with chitosan for enhanced sulfonic dyes removal. Diamond and Related Materials, 155, 112345

   https://doi.org/10.1016/j.diamond.2025.112345

9. Rahman, F. (2025). Trimetallic magnetic nano-composite: A proficient heterogeneous Fenton-like catalyst for methylene blue and paracetamol degradation. Inorganic Chemistry Communications, 178, 114570. https://doi.org/10.1016/j.inoche.2025.114570

10. Hassan, S. S. M., El-Shalakany, H. H., Fathy, M. A., & Kamel, A. H. (2024). A magnetic macroporous α-Fe_2O_3/Mn_2O_3 nanocomposite as an efficient adsorbent for simple and rapid removal of Pb(II) from

wastewater and electronic waste leachate. Environmental Science and Pollution Research, 31, 65648–65660. https://doi.org/10.1007/s11356-024-35452-7

11. Farooq, M., Irfan, M., Almuta, B. S., Shujah, S., Kashita, E., & Amami, M. (2025). Novel Ag-CuO nanocomposites for enhanced lead removal: Structural and adsorption features via green synthesis approach using Capparis decidua plant extract. Microchemical Journal, 216, 114525. https://doi.org/10.1016/j.microc.2025.114525

12. Sabzevari, M., Cree, D. E., & Wilson, L. D. (2018). Graphene oxide—chitosan composite material for treatment of a model dye effluent. ACS Omega, 3(10), 13045–13054

    https://doi.org/10.1021/acsomega.8b01871

13. Yang, X., Tu, Y., Li, L., Shang, S., & Tao, X. (2010). Well-dispersed chitosan/graphene oxide nanocomposites. ACS Applied Materials & Interfaces, 2(6), 1707–1713. https://doi.org/10.1021/am100222m

14. Prasanna, K., & Natarajan, R. (2019). A comprehensive review of applications of magnetic graphene oxide based nanocomposites for sustainable water purification. Journal of Environmental Management, 231, 622–634. https://doi.org/10.1016/j.jenvman.2018.10.063

15. Yusuf, M., Elfghi, F. M., Zaidi, S. A., Abdullah, E. C., & Khan, M. A. (2015). Applications of graphene and its derivatives as an adsorbent for heavy metal and dye removal: A systematic and comprehensive overview. RSC Advances, 5(64), 50392–50420. https://doi.org/10.1039/C5RA07223A

16. Chowdhury, S., & Balasubramanian, R. (2014). Recent advances in the use of graphene-family nanoadsorbents for removal of toxic pollutants from wastewater. Advances in Colloid and Interface Science, 204, 35–56. https://doi.org/10.1016/j.cis.2013.12.005

17. Adeleye, A. S., Conway, J. R., Garner, K., Huang, Y., Su, Y., & Keller, A. A. (2016). Engineered nanomaterials for water treatment and remediation: Costs, benefits, and applicability. Chemical Engineering Journal, 286, 640–662. https://doi.org/10.1016/j.cej.2015.10.105

18. Anjum, M., Miandad, R., Waqas, M., Gehany, F., & Barakat, M. A. (2019). Remediation of wastewater using various nano-materials. Arabian Journal of Chemistry, 12(8), 4897–4919. https://doi.org/10.1016/j.arabjc.2016.10.004

19. Bagheri, H., Afkhami, A., & Noroozi, A. (2019). Development of ternary nanoadsorbent composites of graphene oxide, activated carbon, and zero-valent iron nanoparticles for food applications. Food Science & Nutrition, 7(9), 2827–2837. https://doi.org/10.1002/fsn3.1080

20. Allam, B. K., Musa, N., Debnath, A., Usman, U. L., & Banerjee, S. (2021). Recent developments and application of bimetallic based materials in water purification. Environmental Challenges, 5, 100405. https://doi.org/10.1016/j.envc.2021.100405

21. Wang, P., Fu, F., & Liu, T. (2021). A review of the new multifunctional nano zero-valent iron composites for wastewater treatment: Emergence, preparation, optimization and mechanism. Chemosphere, 285, 131435. https://doi.org/10.1016/j.chemosphere.2021.131435

22. Bayat, M., Nasernejad, B., & Falamaki, C. (2021). Preparation and characterization of nano-galvanic bimetallic Fe/Sn nanoparticles deposited on talc and its enhanced performance in Cr(VI) removal. Scientific Reports, 11(1), 7715. https://doi.org/10.1038/s41598-021-87106-0

23. Le, T. T. N., Le, V. T., Dao, M. U., Nguyen, Q. V., Vu, T. T., Nguyen, M. H., Tran, D. L., & Le, H. S. (2019). Preparation of magnetic graphene oxide/chitosan composite beads for effective removal of

heavy metals and dyes from aqueous solutions. Chemical Engineering Communications, 206(10), 1337–1352. https://doi.org/10.1080/00986445.2018.1558215

24. Tarekegn, M. M., & Balakrishnan, R. M. (2021). Nano zero valent iron (nZVI) particles for the removal of heavy metals (Cd^{2+}, Cu^{2+} and Pb^{2+}) from aqueous solutions. RSC Advances, 11(30), 18539–18551. https://doi.org/10.1039/D1RA01427G

25. Wang, Y., Wang, L., & Li, Y. (2018). Removal of Pb(II) from aqueous solutions by Phytolacca americana L. biomass as a low cost biosorbent. Arabian Journal of Chemistry, 11(1), 99–110. https://doi.org/10.1016/j.arabjc.2015.06.011

26. Manzoor, K., Ahmad, M., & Zafar, M. N. (2019). Removal of Pb(II) and Cd(II) from wastewater using arginine cross-linked chitosan-carboxymethyl cellulose beads as green adsorbent. RSC Advances, 9(14), 7890–7902. https://doi.org/10.1039/C9RA00356H

27. Gebru, K. A., & Das, C. (2016). Removal of Pb(II) and Cu(II) ions from wastewater using composite electrospun cellulose acetate/titanium oxide (TiO_2) adsorbent. Journal of Water Process Engineering, 16, 1–13. https://doi.org/10.1016/j.jwpe.2016.11.008

28. Wu, J., Wang, T., Zhang, Y., & Pan, W. P. (2020). A novel modified method for the efficient removal of Pb and Cd from wastewater by biochar: Enhanced the ion exchange and precipitation capacity. Science of the Total Environment, 754, 142150. https://doi.org/10.1016/j.scitotenv.2020.142150

29. Zhang, X., Lin, S., Chen, Z., Megharaj, M., & Naidu, R. (2010). Removal of Pb(II) from water using synthesized kaolin supported nanoscale zero-valent iron. Chemical Engineering Journal, 163(3), 243–248. https://doi.org/10.1016/j.cej.2010.07.056

30. Lalmi, A., Bouhidel, K. E., & Zertal, A. (2018). Removal of lead from polluted waters using ion exchange resin with $Ca(NO_3)_2$ for elution. Hydrometallurgy, 178, 287–293. https://doi.org/10.1016/j.hydromet.2018.05.009

31. Waly, S. M., El-Wakeel, S. T., & El-Shahat, M. F. (2021). Efficient removal of Pb(II) and Hg(II) ions from aqueous solution by amine and thiol modified activated carbon. Journal of Saudi Chemical Society, 25(7), 101296. https://doi.org/10.1016/j.jscs.2021.101296

32. Zou, X., & Zhang, Y. (2015). Noble metal-free hydrogen evolution catalysts for water splitting. Chemical Society Reviews, 44(15), 5148–5180. https://doi.org/10.1039/C4CS00448E

33. Zhang, Y., Zhang, S., & Chung, T. S. (2015). Nanocomposite membranes for water purification. Advanced Materials, 27(6), 990–1004. https://doi.org/10.1002/adma.201403784

34. Shannon, M. A., Bohn, P. W., Elimelech, M., Georgiadis, J. G., Mariñas, B. J., & Mayes, A. M. (2008). Science and technology for water purification in the coming decades. Nature, 452(7185), 301–310. https://doi.org/10.1038/nature06599

35. Ali, I. (2012). New generation adsorbents for water treatment. Chemical Reviews, 112(10), 5073–5091. https://doi.org/10.1021/cr300133d

36. Crini, G., & Lichtfouse, E. (2019). Advantages and disadvantages of techniques used for wastewater treatment. Environmental Chemistry Letters, 17(1), 145–155. https://doi.org/10.1007/s10311-018-0785-9

37. Wang, J., & Chen, C. (2009). Biosorbents for heavy metals removal and their future. Biotechnology Advances, 27(2), 195–226. https://doi.org/10.1016/j.biotechadv.2008.11.002

38. Ho, Y. S., & McKay, G. (1999). Pseudo-second order model for sorption processes. Process Biochemistry, 34(5), 451–465. https://doi.org/10.1016/S0032-9592(98)00112-5

39. Langmuir, I. (1918). The adsorption of gases on plane surfaces of glass, mica and platinum. Journal of the American Chemical Society, 40(9), 1361–1403. https://doi.org/10.1021/ja02242a004

40. Liu, X., Ma, R., Wang, X., Ma, Y., Yang, Y., Zhuang, L., & Zhu, G. (2019). Graphene oxide-based materials for efficient removal of heavy metal ions from aqueous solution: A review. Environmental Science: Nano, 6(11), 3171–3191. https://doi.org/10.1039/C9EN00983C

41. Reddy, D. H. K., & Yun, Y. S. (2016). Spinel ferrite magnetic adsorbents: Alternative future materials for water purification? Coordination Chemistry Reviews, 315, 90–111. https://doi.org/10.1016/j.ccr.2016.01.012

42. Georgakilas, V., Tiwari, J. N., Kemp, K. C., Perman, J. A., Bourlinos, A. B., Kim, K. S., & Zboril, R. (2016). Noncovalent functionalization of graphene and graphene oxide for energy materials, biosensing, catalytic, and biomedical applications. Chemical Reviews, 116(9), 5464–5519. https://doi.org/10.1021/acs.chemrev.5b00620

43. Xu, C., Wang, K., Zhang, J., & Liu, X. (2015). Magnetic graphene oxide/chitosan composite for removal of methylene blue from aqueous solution. Journal of Colloid and Interface Science, 454, 178–184. https://doi.org/10.1016/j.jcis.2015.05.018

44. Rana, M., Hao, B., Mu, L., Chen, L., & Gell, P. C. (2016). Development of chitosan-based nanocomposites for water treatment. Carbohydrate Polymers, 145, 204–212. https://doi.org/10.1016/j.carbpol.2016.03.032

45. Zubair, M., Ullah, A., & Ahmad, I. (2020). Recent advances in chitosan-based nanocomposites for water purification. International Journal of Biological Macromolecules, 164, 2672–2686. https://doi.org/10.1016/j.ijbiomac.2020.08.140